Journal of Inorganic and General Chemistry
ZAAC
Zeitschrift für anorganische und allgemeine Chemie
DOI: 10.1002/zaac.202000295
ARTICLE

Catalytic Effect of Green CuO Nanoparticles on the Thermal Decomposition Kinetics of Ammonium Perchlorate

Abdenacer Benhammada,[a,b] Djalal Trache,*[a] Salim Chelouche,[a] and Abderrahmane Mezroua[a]

Abstract. In the present work, a green synthesis of copper oxide nanoparticles (CuO NPs) has been performed through a precipitation method using three different copper precursors and sylvestrys leaf extract as a capping agent. Morphology and structure of the obtained CuO NPs were confirmed by X-ray diffraction (XRD), ultraviolet-visible (UV/Vis), Fourier transform infrared (FT-IR) and Raman spectroscopy, as well as scanning electron microscopy (SEM). Moreover, their thermal behavior and catalytic performance were studied using thermogravimetry (TG) and differential scanning calorimetry (DSC). Four isoconversional kinetic methods have been applied to the DSC data obtained at different heating rates in order to determine the kinetic triplets. The results showed that the introduction of CuO NPs has noticeably lowered the thermal decomposition temperature by 91.7, 89.9, and 83.0 °C, and increased the exothermic enthalpy by 1053, 832, and 962 J·g^{-1} for AP-CuO-S, AP-CuO-N, and AP-CuO-Cl, respectively. Furthermore, CuO NPs were found to reduce the activation energy of AP decomposition. Besides that, ammonium perchlorate decomposes following different reaction models g(α), depending on the decomposition stage and the addition of CuO NPs. These results indicate further that the green synthesized CuO nanoparticles are promising ballistic modifiers for composite solid propellants.

1 Introduction

Ammonium perchlorate (AP) has been extensively used as the most common oxidizer for composite solid propellant (CSPs) for several decades due to its outstanding properties.[1] Except its toxicity ,[2] AP has a good compatibility with other solid propellant components, and presents excellent performance.[3] AP (NH_4ClO_4) is an inorganic crystalline salt composed of perchlorate anion (ClO_4^-) and ammonium cation (NH_4^+). It has, indeed, a high oxidizing potential, which makes it suitable for high performance solid propellants.[4] Owing to its crucial importance in propellant formulations, the study of its thermal decomposition behavior, is of a particular interest and attracted much attention from the scientific community for several decades. Nevertheless, this decomposition is found complex, and depends on several aspects, mainly, the experimental conditions, the thermal history of the crystal, and the presence of defects.[5] Although different theoretical and experimental results dealing with the decomposition of AP have been reported in the literature, it undergoes a reversible crystallographic transition from low-temperature orthorhombic structure to a cubic structure at 240 °C,[6] followed by two decomposition steps[3a,6] with an intermediate regime between the two.[5c] The first irreversible decomposition step, named, low-temperature decomposition (LTD), occurs below 300 °C[1a,7] whereas the second decomposition process at a higher temperature (HTD) is observed within the range of 440–450 °C.[8]

To tailor and improve the decomposition of AP what can enhance the performance of the corresponding solid propellant, the incorporation of small amount of combustion catalysts is considered as an effective approach.[9] Owing to their nanometric size and high surface area, metal oxides (MO) nanoparticles are extensively reported as efficient additives and are applied as burning rate modifiers or catalysts for the thermal decomposition of energetic materials.[10] Recently, various metal oxide nanoparticles, including CuO, Fe_2O_3, Co_3O_4, MnO_2, etc., have been investigated as catalysts for AP decomposition.[11] The catalytic effect of such transition metal oxides on the thermal decomposition of AP was revealed to be sensitive to the nature of metal, morphology and microstructure.[12] For instance, the following catalytic order of some MO has been found Mn_2O_3>CuO>Fe_2O_3>Cr_2O_3.[5b] On the other hand, the thermal decomposition as well as the energy output of AP can be adapted through the addition of several MO.[9] For example, the incorporation of 2 wt.-% of NiO nanoparticles increases the heat of decomposition of AP by 900 J·g^{-1}, and decreases the decomposition temperature by 93 °C.[13]

Chen et al. demonstrated the high catalytic effect of $CoFe_2O_4$ on AP thermal decomposition.[10a] The coated α-Fe_2O_3 with amorphous carbon seems to have an interesting catalytic effect on the decomposition of AP for which a decrease of 109 °C in the thermal decomposition temperature is found.[14] In another work, the addition of 0.5 wt.-% MgO and 2 wt.-% ZnO, separately, revealed a notable effect on the reduction of both HTD and Ea of AP, where the activation energy was lowered by 102 kJ·mol^{-1} and 144 kJ·mol^{-1}, respectively.[1a] Some metal coordination compounds prepared using *N*,*N*-bis[1H-tetrazol-5-yl]amine (BTA) and metals (Cu, Na, Zn, Co, Fe) exhibit high catalytic performance on AP thermal de-

* Dr. D. Trache
Fax: +213-21863204
E-Mail: djalaltrache@gmail.com
* Energetic Materials Laboratory
Teaching and Research Unit of Energetic Processes
Ecole Militaire Polytechnique
BP 17, 16046, Bordj El-Bahri, Algiers, Algeria
* Ecole Nationale Préparatoire Aux Etudes d'Ingénieur
Badji-Mokhtar, ENPEI
BP 5, 16013, Rouiba, Algiers, Algeria

composition by reducing HTD temperature by 84.6 °C–125.6 °C, according to the metal nature, with a released energy of 2474–3424 J·g^{-1}, at a heating rate of 10 K·min^{-1}.[15] Interesting catalytic performance of mesoporous graphitic carbon nitride/CuO (mpg-C_3N_4/CuO) nanocomposites on thermal decomposition of AP has also been reported by *Xu* et al., which are assigned to the homogeneous structure and large specific surface area of the prepared nanocomposites.[16] Besides that, the development of a suitable ballistic modifier for the thermal decomposition of ammonium perchlorate remains hot topic research, which requires further activities to find effective ballistic additives.

Copper oxide nanoparticles (CuO NPs), as a p-type semiconductor, have attracted much attention due to their physicochemical properties, which strongly depend on their size, shape and structure.[17] Broadly, CuO NPs have a wide range of applications such as batteries ,[18] new rechargeable lithium-ion batteries (LIBs) ,[19] bio-sensors,[20] gas sensors ,[21] catalysis ,[22] and energetic materials.[23] Several chemical synthetic protocols have been used for the preparation of CuO NPs such as electrochemical methods, solid-state thermal reaction, hydrothermal reaction, sonochemical and microwaves irradiations.[17,24] However, the chemical reaction methods commonly involve the utilization of toxic chemicals, especially capping agents, which can be absorbed on the surface of the synthesized nanoparticles. Therefore, various alternative ecofriendly approaches based on the green concepts have been recently developed to produce CuO NPs, with better features.[25]

It has been proven that the addition of CuO to AP effectively improves its thermal decomposition. Indeed, the incorporation of 2 wt.-% of sphere-like CuO NPs was found to lower the temperature of the thermal decomposition and the Ea by 115 °C and 111 kJ·mol^{-1}, respectively.[26] Likewise, the physical mixing of AP with CuO chrysalis-like morphology at a ratio of 98–2 wt.-% lead to a significant decrease of the HTD by 85 °C.[27] whereas CuO/AP mixture prepared following solvent and non-solvent process diminished the HTD temperature by 90 °C, thus confirming the efficiency of this latter, which improved the catalytic effect of CuO.[28] Recently, it was demonstrated that the catalytic efficiency of the thermal decomposition AP has been significantly improved by the addition of CuO hollow microspheres rather than CuO microparticles and CuO nanoparticles.[29] *Xu* et al. have reported that the addition of 2 wt.-% of mesoporous graphitic carbon nitride-CuO nanocomposites decreased the thermal decomposition of AP by 118.5 °C.[16] In another work, a green synthesis of CuO NPs using Calotropis gigantea plant has been performed and their catalytic effect on the thermal decomposition of AP has been assessed as well.[11b] The authors claimed that the green synthesized CuO NPs displayed a better catalytic effect on the thermal decomposition of AP compared to the MO prepared by the common chemical method. In another work, multichanneled hierarchical porous nanocomposite of CuO and carbonized butterfly wing (CuO/CBW) exhibited excellent catalytic activity on thermal decomposition of AP by reducing the thermal decomposition temperature from 429.1 °C to 340.8 °C, and increasing the released energy by 1586 J·g^{-1}.[30]

To the best of our knowledge, there is no paper dealing with the investigation of the effect of CuO NPs, prepared from different metal precursors using a green capping agent, on the thermal decomposition of AP. This work reports the synthesis and characterization of CuO nanoparticles by a green precipitation method using leaf extract of Malva sylvestris, as stabilizing agent and three different copper precursors. The prepared CuO nanoparticles were deeply characterized using X-ray diffraction (XRD), ultraviolet-visible (UV/Vis), Fourier transform infrared (FT-IR), and Raman spectroscopy as well as scanning electron microscopy (SEM). Afterwards, AP and CuO NPs mixtures were prepared and analyzed by DSC and TG to highlight the effect of the synthetized CuO NPs on the thermal decomposition characteristic parameters of AP. Subsequently, four isoconversional integral models, namely, *it*-KAS (iterative Kissinger-Akahira-Sunose), *it*-FWO (iterative Flynn-Wall-Ozawa),, TAS (Trache–Abdelaziz–Siwani), and Vyazovkin's equation were applied on the DSC data, obtained at different heating rates, to accurately evaluate the kinetic triplet, viz., the activation energy (E_a), the pre-exponential factor [log(A)], and the most probable reaction model [$g(\alpha)$]. In the light of the obtained, conjointly with those reported elsewhere, a Scheme of decomposition mechanism for the AP was proposed.

2 Experimental Section

CuO nanoparticles were synthesized by a precipitation method. First, Malva sylvestris leaf extract was prepared using an aqueous extraction by heating at 80 °C for 10 min, followed by a filtration and a centrifugation steps. Then, 40 mL of plant aqueous extract was added to a 0.05 M copper precursor solution prepared from copper(II) nitrate trihydrate ($Cu(NO_3)_2{\cdot}3H_2O$), copper(II) chloride dehydrate ($CuCl_2{\cdot}2H_2O$), and copper(II) sulfate pentahydrate ($CuSO_4{\cdot}5H_2O$) for which the final products were noted CuO-N, CuO-Cl and CuO-S, respectively. Each mixture was heated at 90 °C for 30 min whilst stirring. At this specific temperature, 0.1 M aqueous solution of NaOH was added dropwise to the mixture until reaching a pH of 11. The obtained precipitate was centrifuged, washed several times with absolute ethanol and distilled water, and then dried at 70 °C in oven for 6 h. Finally, the produced powder was annealed at 550 °C for 4 h.

To prepare homogeneous CuO-AP nanocomposites, 5 wt.-% of CuO NPs were dispersed in 50 mL of acetone by sonication for 10 min to avoid their agglomeration. Then, 95 wt.-% of AP were added gradually whilst stirring for 2 h. Finally, the obtained mixture was dried at room temperature, mixed in agate mortar, and conserved for further analyses.

X-ray diffraction analyses were performed on PANalytical X'Pert PRO X-ray diffractometer using Cu anode K_α radiation (λ = 1.54 Å), a current of 40 mA and an accelerating voltage of 45 kV. Scanning electron microscope (SEM) images were obtained on a JEOLJEM200CX instrument with an accelerating voltage of 2 kV. To get more insights on the chemical structure of the catalysts, the FTIR experiments were carried out by Bruker-vertex70 in wavelength range of 400–4000 cm^{-1}, whereas Raman spectroscopy analyses were conducted on thermo Scientific DXR with a laser excitation wave of 532 nm within the range of 1000 and 100 cm^{-1}. Shimadzu UV/Vis (UV-1800) Spectrophotometer was used to study the vibrational properties the synthesized samples.

The thermal behavior of the prepared nanocomposites were performed using, respectively, a thermogravimetry analysis TG (Perkin–Elmer TGA Q500 V20.13) at a heating rate of 10 K·min^{-1} from 180 °C to 420 °C, and a differential scanning calorimetry (Perkin–Elmer DSC8000) at the heating rates of 5, 10, 15 and 20 K·min^{-1} from room temperature to 450 °C. The thermal analysis measurements were carried out in a nitrogen atmosphere at a flow rate of 20 mL·min^{-1}.

As stated by the International Confederation for Thermal Analysis and Calorimetry (ICTAC) kinetics committee, isoconversional kinetic analysis performed on non-isothermal data obtained at multiple heating rates provides accurate values of the kinetic parameters.[31] Therefore, in the present work, based on the DSC data, four isoconversional integral method, namely, TAS (Trache–Abdelaziz–Siwani), Vyazovkin's equation (VYA), *it*-FWO (iterative Flynn-Wall-Ozawa) and *it*-KAS (iterative Kissinger-Akahira-Sunose were used to determine the activation energy Ea, pre-exponential factor log(A) and the most probable mechanism for the decomposition reaction g(α) of the elaborated systems. The calculations were made using a compiled program on MATLAB.

3 Results and Discussions

3.1 Characterization of CuO NPs

Figure 1a shows the XRD patterns for the prepared CuO NPs. The XRD diffraction peaks could be attributed to the monoclinic crystalline phase of the CuO (Tenorite) with a space group *C*2/*c* (JCPDS 00–048–1548), unveiling the high crystalline nature of CuO NPs. Likewise, no diffraction peaks, which can be attributed to the impurities from the synthesis procedure like $Cu(OH)_2$, as intermediate product, or cupper precursors were observed, thus confirming the purity of the as-prepared copper oxide nanoparticles. Besides, the sharpness and broadening of of CuO-N and CuO-Cl diffraction peaks, reveal a higher crystallinity compared to CuO-S sample. The crystallite size diameters, estimated using Debye–Scherrer's equation [Equation (1] are found equal to 28 nm, 25 nm, and 20 nm for CuO-Cl, CuO-N, and CuO-S, respectively:

$$d = \frac{k\,\lambda}{\beta \cos\theta} \tag{1}$$

where d stands for the crystallite size diameter, k is the shape factor (0.94), λ is the wavelength of Cu-K_α anode radiation (λ = 1.54 Å), whereas β_{hkl} refers to the full width at the half maxima value (FWHM) in radians, and θ corresponds to the scattering angle of the main reflection peak.

The FTIR spectra obtained for the synthesized CuO NPs (Figure 1b) indicating similar chemical composition. The peaks at 1642 and 1483 cm^{-1} are ascribed to the bending mode of O–H ,[22] whereas the adsorption peak at around 3414 cm^{-1} is attributed to the stretching vibrational mode of

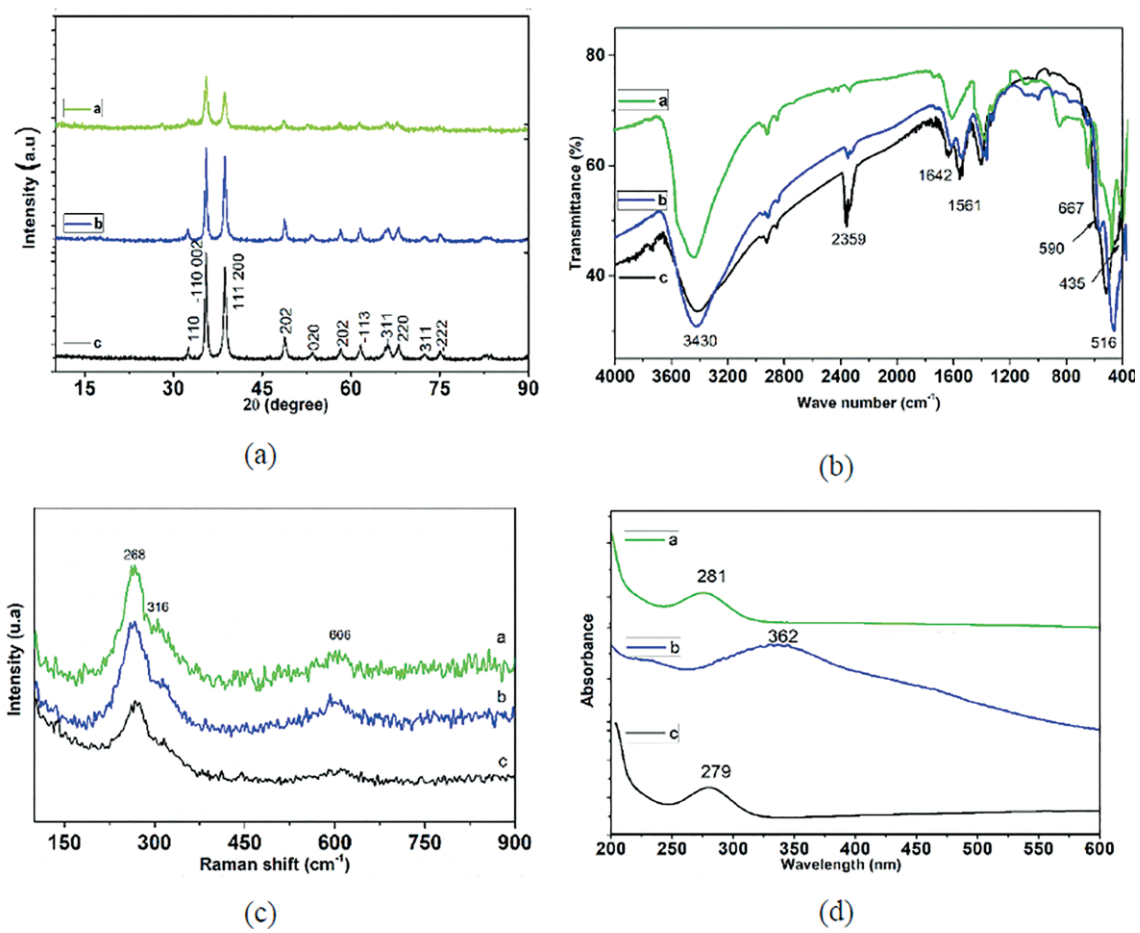

Figure 1. (a) XRD patterns of CuO NPs, (b) FTIR spectra of the prepared CuO nanoparticles, (c) Raman spectra of the prepared CuO, (d) UV/Vis spectra of CuO nanoparticles. CuO-S (a), CuO-Cl (b), and CuO-N (c).

O–H bond of the water molecules.[32] The bands at 2359 and 1350 cm^{-1} are, respectively, assigned to the asymmetric and symmetric stretching of the adsorbed CO_2.[33] The bands at 670–430 cm^{-1} corresponded to stretching vibrational modes of metal–oxygen (Cu–O) bonds.[34] As a complementary to FTIR analysis, Raman spectra of the as-prepared CuO NPs are depicted in Figure 1c. It can be seen that the main Raman phonons bands of CuO nanocrystals appeared as expected at 270, 320, and 610 cm^{-1}.[35]

The optical properties of the prepared copper oxide nanoparticles were determined using UV/Vis spectroscopy. The obtained spectra, recorded between 200 and 600 nm, are displayed in Figure 1d. The observed adsorption peak at 280 nm for CuO–S and CuO–N, and at 360 nm for CuO–Cl indicates the formation of copper oxide at nono-sized diameter. Meanwhile the Plasmon surface resonance (PSR) bands appear when the particle size is less than the incident radiation wavelength, and shift to higher values with the increase of the particle size.[36] The typical SEM micrographs of the prepared CuO NPs are shown in Figure 2. It can be observed that the employed precursors do not affect the granular shape of CuO, which are nanometric in size, but agglomerated because of the high surface energy of the MO particles at nanoscale.

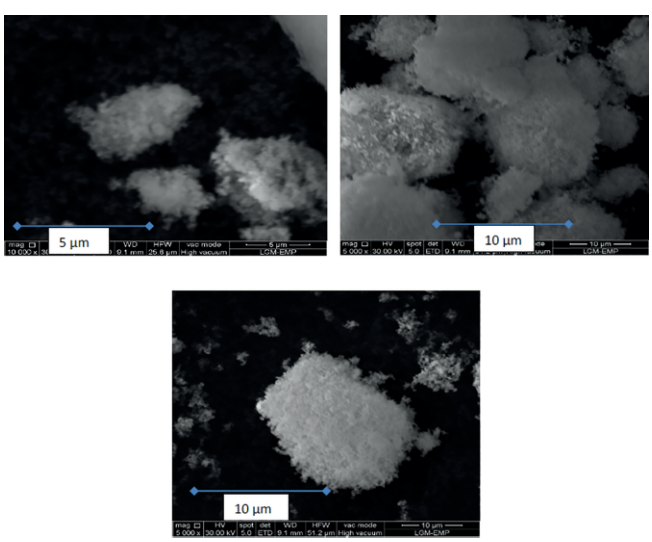

Figure 2. SEM images of CuO nanoparticles (1): CuO-N, (2) CuO-S, (3) CuO-Cl.

3.2 Thermal Behavior of AP/CuO Mixtures

TG and DSC measurements have been conducted to accurately assess the effect of the prepared CuO NPs from different precursors on the thermal behavior of AP. The TG/DTG curves shown in Figure 3, obtained at a heating rate of 10 K·min^{-1}, obviously demonstrated the catalytic effect of the added additives on the thermal decomposition of AP. Similarly to what is reported in literature ,[37] pure AP exhibits three mass loss stages within the temperature range of 200 °C to 400 °C (Figure 3a and b).

The first weight loss of 3.76 % occurred within the range of 275–290 °C is assigned to the low thermal decomposition (LTD). The second one, which is not commonly observed by most researchers, occurred with a weight loss of 20.10 % within the range 295–322 °C, is attributed to the intermediate thermal decomposition (ITD),[37c,38] whereas the last stage, arisen within the range 330–382 °C with a weight loss of 75.75 %, is attributed to the high thermal decomposition (HTD). It was reported that the LTD decomposition is a multiphase decomposition, usually explained by three conflicting theories,[6] involving either (1) an electron transfer from ClO_4^- to NH_4^+ [Equation (2)] proposed earlier by *Bircumshaw* and *Newman*,[39] (2) the breakup of the chlorine–oxygen bond,[5c] or (3) a proton transfer mechanism through the proton transfer from ammonium cation to perchlorate anion ClO_4^-. This latter one, which is adopted nowadays by several researchers, is considered as the most convincing theory.[5c]

$$NH_4^+ + ClO_4^- \rightarrow NH_3 + HClO_4 \quad (2)$$

Using TG-MS hyphenated techniques, *Longuet* and *Gillard*[40] have assumed that the main released gases at LTD decomposition are H_2O, N_2, O_2, Cl_2, N_2O,NO and NO_2, following Equation (3).

$$NH_4ClO_4 \rightarrow ½\ Cl_2 + 1/8\ N_2 + 5/16\ N_2O + 1/8\ NO + 2\ H_2O + 25/32\ O_2 \quad (3)$$

As the temperature increased, the released gases could react with AP and the main evolved gases, corresponding to the HTD decomposition are NO_2, N_2O, O_2, Cl_2, H_2O with a little of NO. The main evolved gases and the most decomposition mechanisms of AP using hyphenated techniques have been reported in our previous work.[37c]

The thermal decomposition of AP supplemented with CuO NPs occurred in one-step, as shown in plots a-e in Figure 3 for which the decomposition parameters process was notably decreased. From TGA/DTG plots, the HTD temperature decreased from 358 °C for pure AP to 319.1 °C, 319 °C and 319.1 °C for AP-CuO-S, AP-CuO-Cl and AP-CuO-N, respectively. The average total weight loss for AP-CuO is around 94.5 %. The remaining amount is probably assigned to the added catalysts.

To further investigate the thermal decomposition of the prepared nanocatalysts/AP mixtures, DSC analyses have been performed at different heating rates, and the obtained curves are shown in Figure 4. All the DSC curves display one endothermic peak at a constant temperature of 243 °C (the onset temperature observed at 240 °C), which is ascribed to the crystallographic transition of AP from an orthorhombic structure to cubic structure.[6] This finding is of paramount importance since it proves that the addition of catalysts did not influence the allotropic transition of AP.[41] Besides, no weight loss was observed at this temperature, as seen in the TG curves. For pure AP (Figure 4a), the DSC curve shows two thermal decomposition stages corresponding, respectively, to the LTD and the HTD decompositions, whereas the thermal decomposition of the catalyzed AP (Figure 4b, c, and d) displays only one-step behavior with a lower decomposition temperature. Indeed, for heating rate of 10 K·min^{-1}, the LTD temperature is

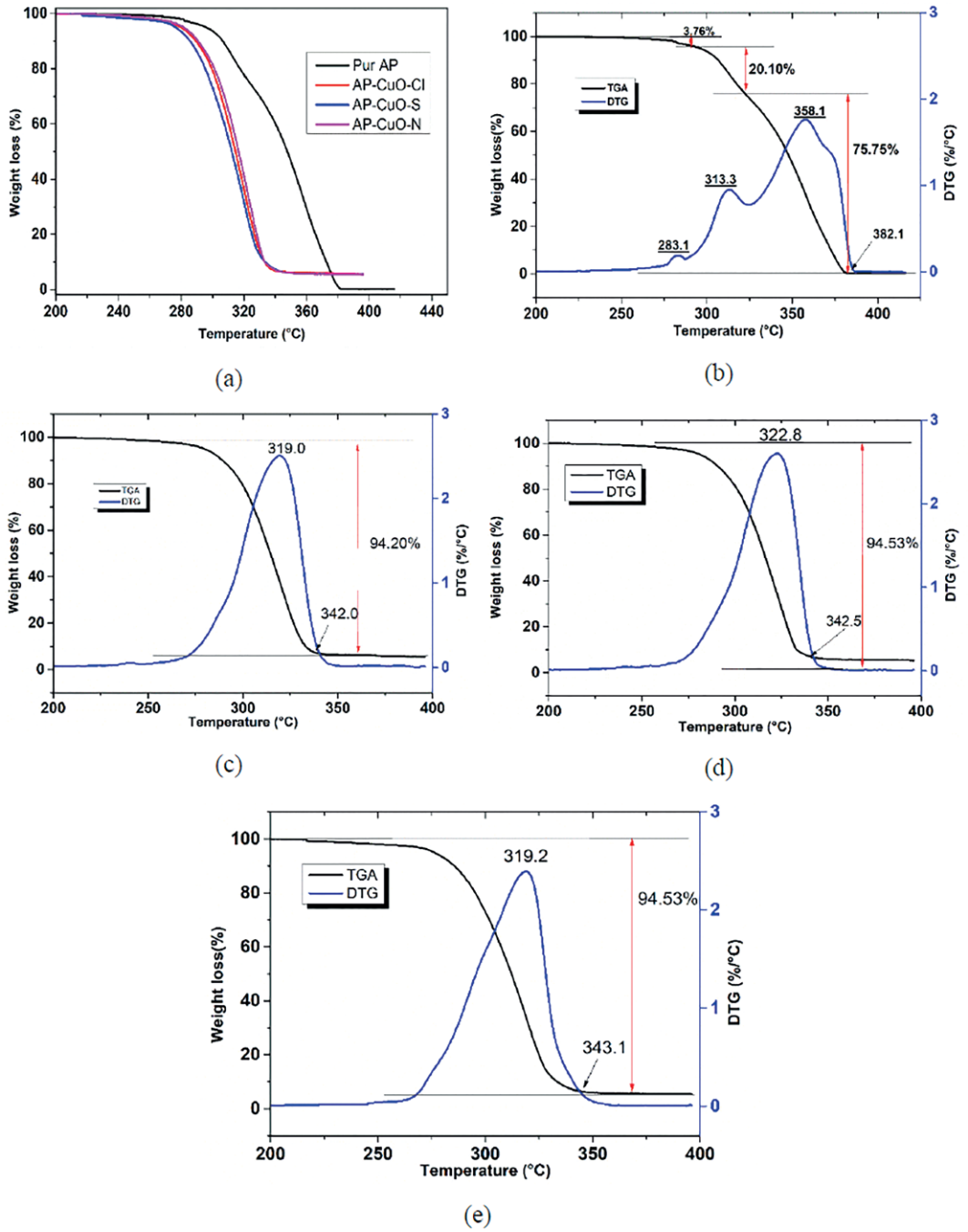

Figure 3. (a) TG curves for AP and AP-CuO systems, and DTG curves (b) pure AP, (c) AP-CuO-Cl, (d) PA-CuO-N and (e) PA-CuO-S.

centered at 312.3 °C and the HTD peak is observed at 415.8 °C for pure AP. It is worthy to note that the ITD stage was not obtained with DSC measurements.[16] After the incorporation of the catalysts to AP, the HTD temperature has been lowered by 91.5, 90.2 and 84.1 °C for CuO–S, CuO–N and CuO–Cl, respectively (Figure 4e). These results prove the good catalytic effect of the prepared CuO NPs on the thermal decomposition of ammonium perchlorate. Otherwise, all the systems exhibit the same trend for which the peak temperature shifts to higher values with the increase of the heating rate (Figure 4 and Figure 5c). This evolution is commonly encountered for energetic materials such as AP,[42] nitrocellulose,[10c] and other energetic composites.[43] On the other hand, the exothermic peaks became sharper with the increase of the heating rates, leading to a faster thermal decomposition.[44]

The catalytic effect of CuO NPs on thermal decomposition of AP was also highlighted through the comparison of the exothermic heat released (ΔH) during the decomposition process, since higher energy release means higher performance for modern rocket applications.[10a] Figure 5a and b show the exothermic energy release at two different heating rates (10 K·min^{-1} and 20 K·min^{-1}). Accordingly, for a heating rate

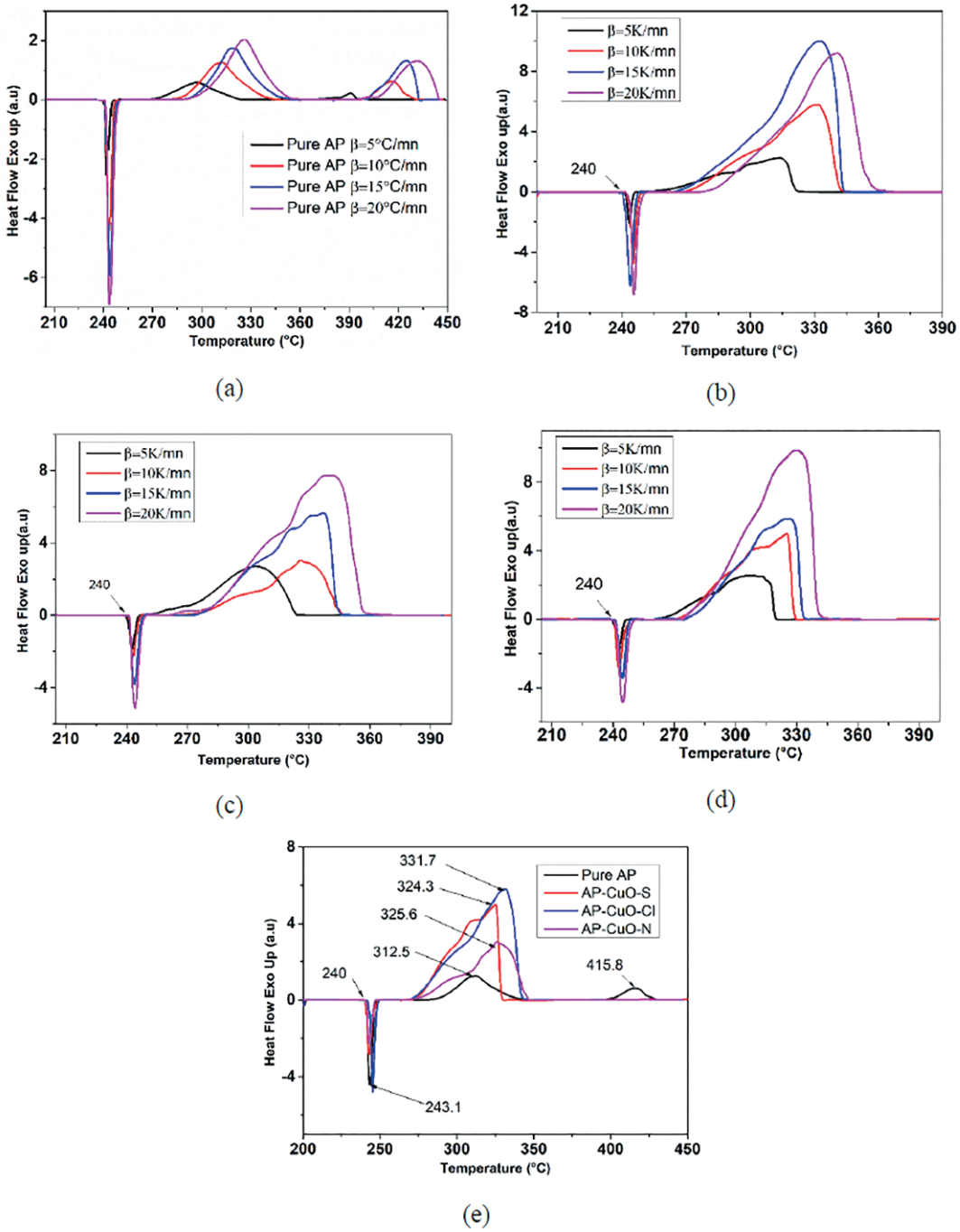

Figure 4. DSC curves of AP at different heating rates: (a) pure AP, (b) AP-CuO-Cl, (c) AP-CuO-N, (d) AP-CuO-S, and (e) superposition of DSC curves at β = 10 K·min^{-1}.

of 10 K·min^{-1}, the overall released energy of AP is 293.1 J·g^{-1}. When 5 wt.-% of CuO NPs was introduced, the HTD energy release increases exceptionally by 1053, 962, and 832 J·g^{-1} for AP-CuO-S, AP-CuO-Cl and AP-CuO-N, respectively, leading to the total decomposition of AP through the improvement of the contact between fuel/oxidizer species of AP. This finding can be easily connected to the better dispersion of CuO within the AP matrix.

In addition, it is worthy to note that this energy release increases to more than 1320 J·g^{-1} at a heating rate of 20 K·min^{-1}. These results suggested that the addition of nanocatalysts to AP promotes the fuel/oxidizer reaction, and hence a great amount of energy is released in short time.[41] Furthermore, this energy release, which can be seen as a pure thermodynamic parameter, is not directly influenced by the addition of catalyst. Moreover, the added catalysts may affect the reaction mechanism or pathway with higher reaction rate. Furthermore, it is well known that some of the main parameters to consider for AP applications are its exothermic energy and its decomposition temperature.[45] The obtained results from the

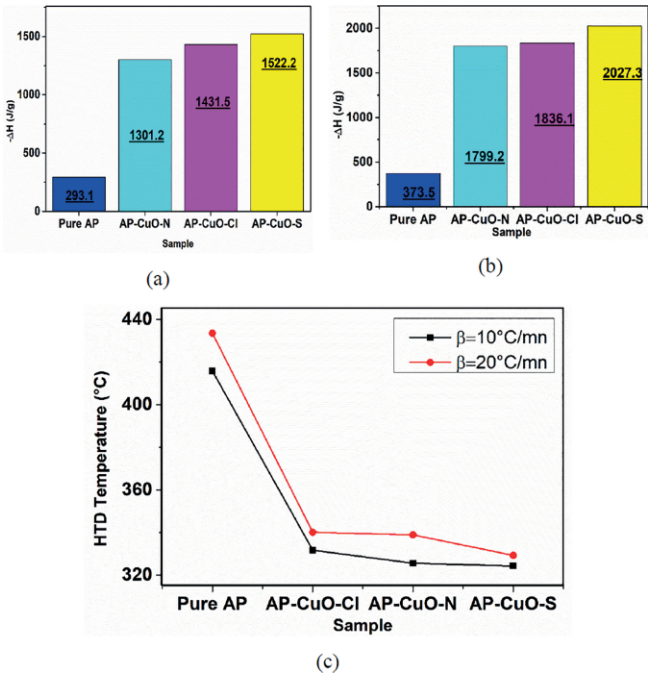

Figure 5. Histograms of exothermic energy release (a) at β = 10 K·min^{-1}, (b) at β = 20 K·min^{-1}, and (c) the corresponding HTD temperature.

thermal analysis, showed a promising catalytic effect of the prepared CuO NPs using Malva sylvestris leaf extract on the thermal decomposition of AP for which the energy release increased and thermal decomposition temperature decreased.[46]

Table 1 presents a comparative survey of the decomposition temperature and energy release of AP with different catalysts reported in the literature compared to the as-prepared CuO NPs. It can be seen that the as-prepared green CuO NPs catalyze effectively the thermal decomposition of AP with higher energy release and lower decomposition temperature than other catalysts such as CuO nanoparticles, hollow mesoporous CuO, CuO powder, CuO-nanorods, CuO microflowers, Cu-Cr-O and Co_3O_4. Furthermore, this catalytic effect was found very close to that from supported metal oxides such as graphene-CuO, mpg-C_3N_4-CuO, which commonly played a synergetic effect of CuO and the catalytic supports,[16] or metal oxalate like FeC_2O_4.[41]

3.3 Evaluation of Kinetic Parameters based on Isoconversional Analysis

Kinetic modeling on data obtained from thermal techniques such as differential scanning calorimetry (DSC) and TG could be a tremendous way to investigate the thermal degradation kinetics of energetic materials. The obtained kinetic parameters allow estimating precisely the impact of the CuO NPs on the energetic barrier and the rate of the decomposition reaction rate, as well as the mechanisms involved. On the other hand, in solid-state kinetics, the application of traditional model- fitting on non-isothermal data can lead to erroneous evaluation of the Arrhenius parameters, which is generated by the use of a statistical approach to select the appropriate model that best fit the chemical reaction.[51] However, the use of the isoconversional approach in both isothermal and non-isothermal kinetics helps to avoid the issues generated from the ambiguous evaluation of the reaction model.[52] Moreover, the use of multiple heating rates is strongly recommended by the International Confederation for Thermal Analysis and Calorimetry (ICTAC) kinetics committee since more reliable kinetic parameters are achieved [31b] Over the years, the isoconversional methodology has spread broadly and proven convincingly its worth for kinetics studies of thermally stimulated processes in energetic materials and other systems.[53,53b,54]

In the present work, the kinetic triplet (activation energy, pre-exponential factor and the most probable reaction model) was determined using four isoconversional models, namely, the iterative equations *it*-KAS (Kissinger–Akahira–Sunose) and *it*-FWO (Flynn–Wall–Ozawa) suggested by *Gao* et al.,[55] Sbirrazzuoli methodology (VYA/CE method) proposed by *Vyazovkin*[31b,56] and TAS (Trache–Abdelaziz–Siwani) method proposed by *Trache* et al.[57] based on modified Coats–Redfern Equation. The details of these methods as well as the isoconversional kinetic analysis could be found in our previous works.[10c,58] All the calculations have been performed on the

Table 1. Comparison of the decomposition temperature and the energy release of different catalysts on AP thermal decomposition.

Sample	Decomposition temperature (DSC)	Heat release /J·g^{-1}	Reference
CuO-S nanoparticles	324.3	1522	This work
CuO-N nanoparticles	325.6	1431	This work
CuO-Cl nanoparticles	331.7	1301	This work
CuO nanoparticles	345.5	1046	[29]
Hollow mesoporous CuO	329.5	1113	[29]
CuO microflowers	353.17	1211	[47]
CuO NPs	341.2	1486	[28]
Graphene-CuO	321.0	1893	[48]
CuO powder (2%)	350.4	1054.5	[37a]
CuO-nanorods (2%)	345.1	994.3	[16]
g-C_3N_4	396.5	834.1	[16]
mpg-C_3N_4-CuO	335.1	1664	[16]
MnC_2O_4	311.0	1223	[41]
FeC_2O_4	393.0	1662	[41]
Cu-Cr-O	346.0	1192	[49]
Co_3O_4	301.8	1042	[50]

DSC data obtained at different heating rates and presented previously. A Matlab interface was designated in order to carry out the computations.

Figure 6 presents the evolution of activation energy E_a with respect to the extent of conversion α, whereas their average values are reported in Table 2. The obtained activation energy values using the four models, namely, it-KAS, it-FWO, TAS and VYA are very close to each other, with lower values for it-FWO, confirming the precision of the performed calculations. The accuracy of the obtained values was confirmed also by the values of the linear correlation coefficient R^2 fluctuating within the range of 0.9134–0.9987, revealing the reliability of the exploitation of isoconversional models in the investigations of thermal decomposition behavior of energetic materials.[58,59] Furthermore, the obtained activation energy dependence on the extent of conversion shows a slight difference trend according the system, and confirms the complexity of the thermal decomposition process of AP. Besides that, Figure 6a indicates three stages for the E_a evolution of the AP decomposition reaction against the conversion extent. More explicitly, the first stage (I) corresponds to an increase of E_a until 130.24 kJ·mol^{-1} for $\alpha < 0.28$. In the second stage (II) ($\alpha = 0.28$–0.88), however, E_a decreases within the range 130.24–117.96 kJ·mol^{-1}, whereas it increases in the last stage (III) (0.88 to the end) from 117.96 to 137.13 kJ·mol^{-1}. Such behavior was previously encountered in other works.[5a,60]

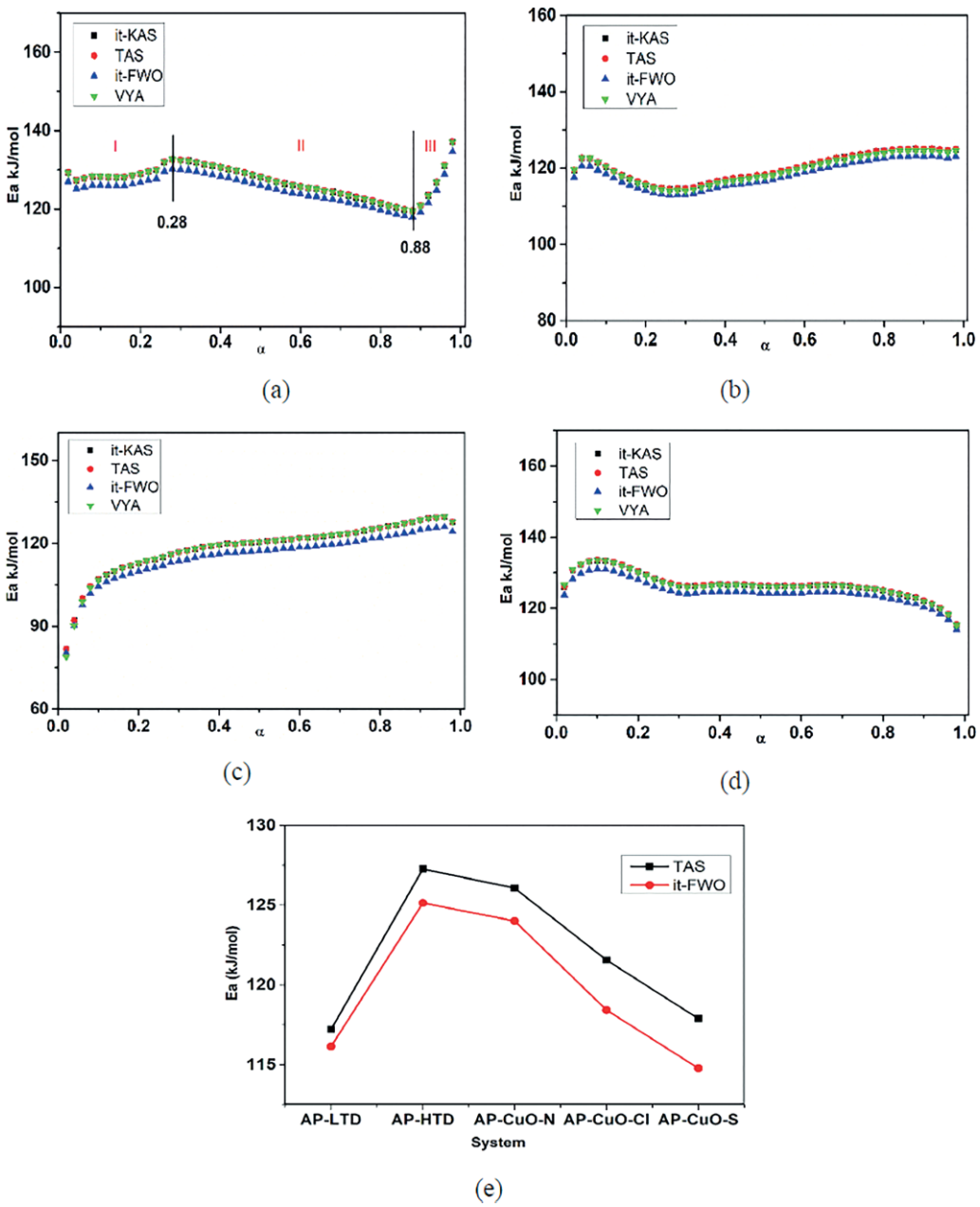

Figure 6. Activation energy E_a dependence on the extent of conversion α: (a) pure AP, (b) AP-CuO-Cl, (c) AP-CuO-S, (d) AP-CuO-N, and (e) comparison of average activation energy using TAS and it-FWO methods.

Table 2. Activation energy E_a, decimal logarithm of the pre-exponential factor log(A) and the most probable mechanism g(α) for the investigated systems.[a)].

System	Isoconversional method		Kinetic parameters E_a /kJ·mol^{-1}	log(A) /S^{-1}	g(α)
Pure AP (LTD)	It-KAS		117.054	6.539	$F_{1/3} = 1–(1–\alpha)^{2/3}$
	It-FWO		116.147	6.5357	$F_{1/3} = 1–(1–\alpha)^{2/3}$
	TAS		117.213	6.622	$G_7 = [1–(1–\alpha)^{1/2}]^{1/2}$
					$G_8 = [1–(1–\alpha)^{1/3}]^{1/2}$
	Vyazovkin/CE	β = 5 K·min^{-1}	117.051	6.473	
	Vyazovkin/CE	β = 10 K·min^{-1}		6.774	
	Vyazovkin/CE	β = 15 K·min^{-1}		6.949	
	Vyazovkin/CE	β = 20 K·min^{-1}		7.075	
Pure AP (HTD)	It-KAS		127.183	8.814	$P_{1/2} = \alpha^{1/2}$
	It-FWO		125.142	8.807	$P_{1/2} = \alpha^{1/2}$
	TAS		127.272	8.892	$P_{1/4} = \alpha^{1/4}$
	Vyazovkin/CE		127.201	8.850	
	Vyazovkin/CE			9.151	
	Vyazovkin/CE			9.328	
	Vyazovkin/CE			9.453	
AP-CuO-S	It-KAS		117.863	8.683	$A_1 = –\ln(1–\alpha)$
	It-FWO		114.777	8.677	$A_1 = –\ln(1–\alpha)$
	TAS		117.892	8.311	$F_{1/2} = 1–(1–\alpha)^{1/2}$
					$F_{1/3} = 1–(1–\alpha)^{2/3}$
	Vyazovkin/CE	β = 5 K·min^{-1}	117.751	8.365	
	Vyazovkin/CE	β = 10 K·min^{-1}		8.546	
	Vyazovkin/CE	β = 15 K·min^{-1}		8.651	
	Vyazovkin/CE	β = 20 K·min^{-1}		8.727	
AP-CuO-N	It-KAS		125.976	8.591	$F_{1/3} = 1–(1–\alpha)^{2/3}$
	It-FWO		124.002	8.585	$F_{1/3} = 1–(1–\alpha)^{2/3}$
	TAS		126.068	8.751	$G_7 = [1–(1–\alpha)^{1/2}]^{1/2}$
					$G_8 = [1–(1–\alpha)^{1/3}]^{1/2}$
	Vyazovkin/CE	β = 5 K·min^{-1}	125.879	8.629	
	Vyazovkin/CE	β = 10 K·min^{-1}		8.931	
	Vyazovkin/CE	β = 15 K·min^{-1}		9.107	
	Vyazovkin/CE	β = 20 K·min^{-1}		9.232	
AP-CuO-Cl	It-KAS		121.458	8.692	$A_2 = [–\ln(1–\alpha)]^{1/2}$
	It-FWO		118.426	8.462	$A_2 = [–\ln(1–\alpha)]^{1/2}$
	TAS		121.556	8.323	$G_7 = [1–(1–\alpha)^{1/2}]^{1/2}$
					$G_8 = [1–(1–\alpha)^{1/3}]^{1/2}$
	Vyazovkin/CE		121.117	8.195	
	Vyazovkin/CE			8.496	
	Vyazovkin/CE			8.672	
	Vyazovkin/CE			8.797	

a) $F_{1/3}$ = chemical reaction, $F_{1/2}$ = contracting cylinder, G_7 and G_8 = other kinetic equations with unjustified mechanism (TAS), $P_{1/2}$ and $P_{1/4}$ = nucleation (power low), A_1 = random nucleation/first order (Mampel), A_1 = random nucleation (Avrami–Erofeev).

After the introduction of copper oxide nanoparticles, different multistep curves were obtained. AP-CuO-S mixture (Figure 6c) exhibits a continuous increase of E_a, whereas AP-CuO-N and Ap-CuO-Cl show a fluctuation of E_a between increase and decrease (Figure 6b and d). Besides, the addition of CuO decreases the activation energy from 127.2 kJ·mol^{-1} for pure AP to 117.75, 125.87 and 121.12 kJ·mol^{-1} for AP-CuO-S, AP-CuO-N and AP-CuO-Cl, respectively, as can be seen Figure 6e. The obtained values of E_a are in good agreement with those reported in the literature.[5a,61] The decrease in the E_a values with the incorporation of the CuO NPs points out their excellent catalytic effect of on thermal decomposition of AP. The highest catalytic effect was observed for CuO-S nanoparticles (Table 3)

The plot of the evolution of pre-exponential factor log(A) with respect to the extent of conversion α, obtained for the four used isoconversional models, is presented in Figure 7. It could be noted that for all the studied systems, the evolution trend of log(A) is close to what is observed for v evolution.

Table 3. Comparison of the activation energy E_a of AP thermal decomposition obtained using different catalysts.

Catalyst	E_a /kJ·mol^{-1} Pure AP	AP+ catalyst	Reference
CuO-S	127.18	117.86	This work
CuO-N	127.18	125.98	This work
CuO-Cl	127.18	121.46	This work
δ-AlOOH	346.29	144.73	[63]
ZnO	154.00	90.80	[61]
CuO	324.24	120.13	[64]
AP / ZnO	280.30	178.70	[1a]
AP / MgO	280.30	136.90	[1a]
AP /g-C_3N_4	216.00	119.80	[8]
AP / CuO	213.40	86.70	[37a]
AP /g-C_3N_4-CuO	213.40	67.60	[37a]
AP / Cu_2O	133.17	112.51	[5a]

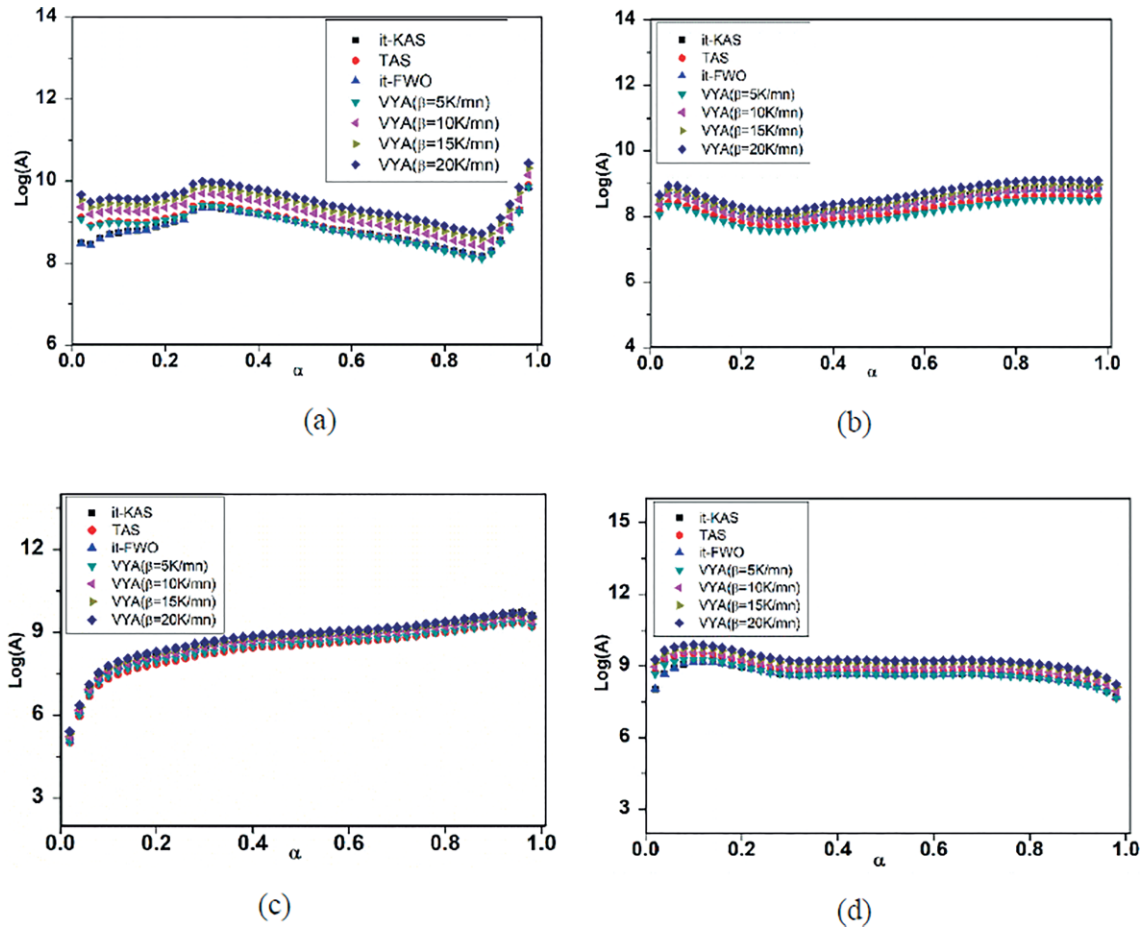

Figure 7. Pre-exponential factor dependence on the extent of conversion α: (a) pure AP, (b) AP-CuO-Cl, (c) AP-CuO-S, (d) AP-CuO-N.

Table 4. Compensation parameters *a* and b using TAS and VYA/CE methods.

System			*a* /mol·J^{-1}	*b*	R^2
Pure AP (HTD)	TAS		0.1883 ± 0.0018	–6.8186 ± 0.0115	0.99512
	VYA/CE	β = 5 K·min^{-1}	0.18247 ± 0.0014	–6.4546 ± 0.0011	0.99968
		β = 10 K·min^{-1}	0.18247 ± 0.0014	–5.7639 ± 0.0011	0.99968
		β = 15 K·min^{-1}	0.18247 ± 0.0014	–5.3564 ± 0.0011	0.99968
		β = 20 K·min^{-1}	0.18247 ± 0.0014	–5.0695 ± 0.0011	0.99968
AP-CuO-S	TAS		0.22403 ± 0.0034	–9.3612 ± 0.3237	0.99853
	Vyazovkin/CE	β = 5 K·min^{-1}	0.20947 ± 0.0257	–6.4314 ± 0.0072	0.99863
		β = 10 K·min^{-1}	0.20947 ± 0.0257	–5.7382 ± 0.0072	0.99863
		β = 15 K·min^{-1}	0.20947 ± 0.0257	–5.3328 ± 0.0072	0.99863
		β = 20 K·min^{-1}	0.20947 ± 0.0257	–5.0451 ± 0.0072	0.99863
AP-CuO-N	TAS		0.23727 ± 0.0042	–9.7624 ± 0.5316	0.99254
	Vyazovkin/CE	β = 5 K·min^{-1}	0.20796 ± 0.0245	–6.3759 ± 0.0072	0.99869
		β = 10 K·min^{-1}	0.20796 ± 0.0245	–5.6828 ± 0.0072	0.99869
		β = 15 K·min^{-1}	0.20796 ± 0.0245	–5.2776 ± 0.0072	0.99869
		β = 20 K·min^{-1}	0.20796 ± 0.0245	–4.9899 ± 0.0072	0.99869
AP-CuO-Cl	TAS		0.19259 ± 0.0020	–4.2461 ± 0.2422	0.99746
	Vyazovkin/CE	β = 5 K·min^{-1}	0.20891 ± 0.0258	–6.4329 ± 0.0072	0.99861
		β = 10 K·min^{-1}	0.20891 ± 0.0258	–5.7398 ± 0.0072	0.99861
		β = 15 K·min^{-1}	0.20891 ± 0.0258	–5.3343 ± 0.0072	0.99861
		β = 20 K·min^{-1}	0.20891 ± 0.0258	–5.0466 ± 0.0072	0.99861

Therefore, lower values of log(A) correspond to lower values of E_a. This similitude of evolution has been evoked in our previous works for nitrocellulose thermal decomposition and could be explained by the compensation effect,[62] which is

represented by a linear correlation between E_a and log(A), following Equation (4):

$$\ln(A) = a\,E_a + b \quad (4)$$

The compensation parameters (a and b) have been determined for the different systems at heating rate of 5, 10, 15 and 20 K·min^{-1}, using TAS and VYA/CE isoconversional models. For each heating rate, the plot of log(A) against E_a allows determining the compensation parameters for which the results are shown in Table 4. As it was already assumed, the good linear correlation coefficient R^2 is higher than 0.99 for all of the investigated systems, confirming the establishment of compensation effects between log(A) and E_a.

3.4 Investigation of the Most Probable Integral Reaction Model g(α)

Based on the forty-one mathematic models reported in our previous work,[57] the most probable model g(α) was determined for each system using the four is conversional methods at different heating rates. Figure 8 displays the evolution of the reaction models with the extent of conversion α, whereas the most probable g(α) models are given in Table 2. The examination of the obtained results indicates that different reaction models could be assigned, according the employed isoconversional method and the considered system.

Based on it-KAS and it-FWO methods, AP decomposes at the LTD according to F1/3 model g(α) = 1–(1–α)$^{2/3}$, which is

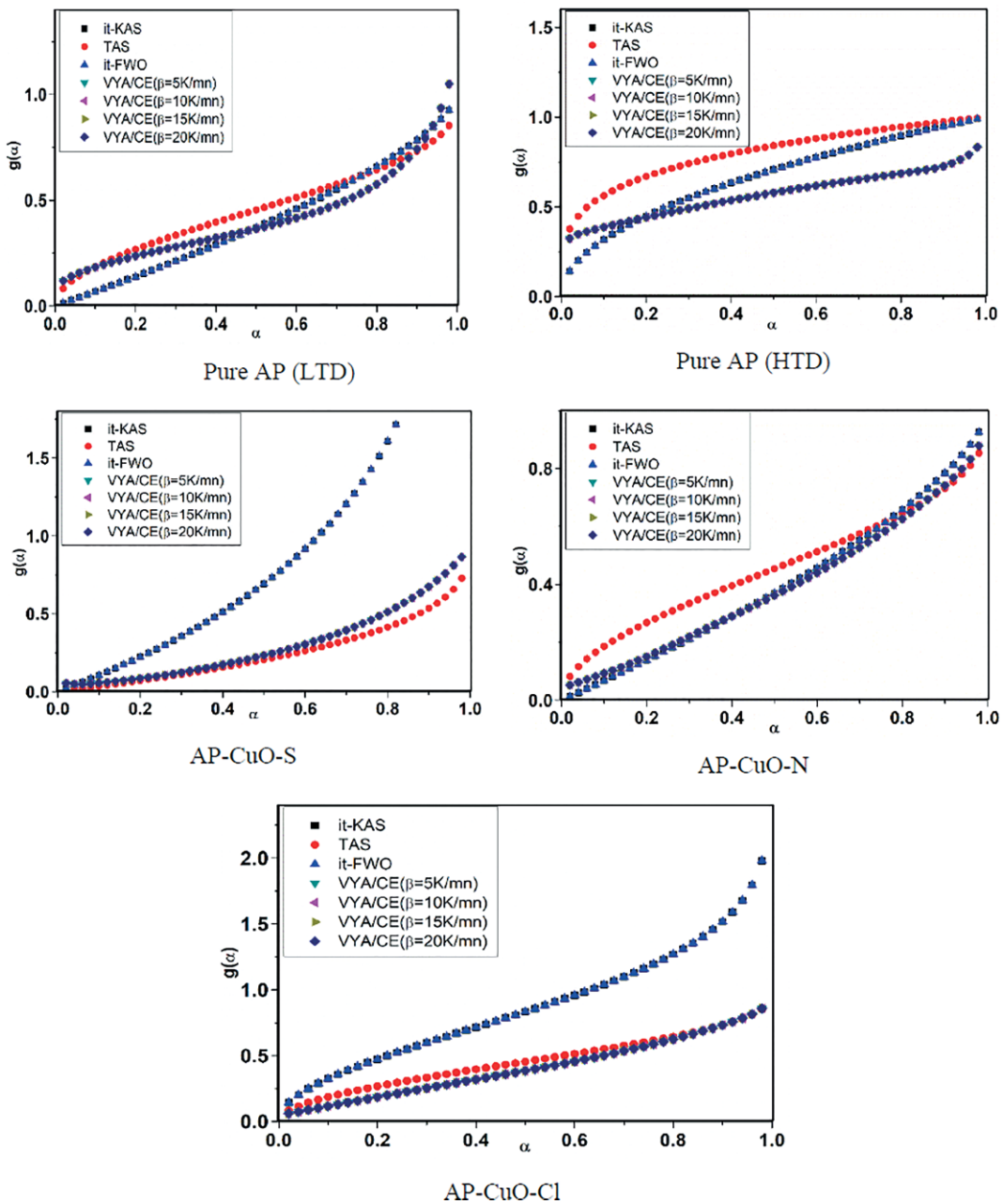

Figure 8. Integral reaction model values evolution as function of α for the investigated systems.

related to the chemical reaction with n^{th} (n = 2/3) reaction order, whereas at HTD, AP appears to decompose following P1/2 model $g(\alpha) = \alpha^{1/2}$, which belongs to a nucleation (Power low) process. However, other models have been obtained for AP supplemented with catalysts. For instance, AP-CuO-S decomposes according A1 model (random nucleation/first order (Mampel)), while AP-CuO-Cl decomposition is governed by A2 model (random nucleation (Avrami-Erofeev), growth, n = 2) and AP-CuO-S followed a F1/3 model. Moreover, TAS method provides G7 and G8, with unjustified mechanism for pure AP at LTD, AP-CuO-Cl and AP-CuO-N against F1/3 model or F1/2 (contracting cylinder) for AP-CuO-S and P1/4 model for pure AP at HTD thermal decomposition. The VYA/CE provides only numerical values. Similar results have been obtained by *Ramdani* et al.[5a] who assumed different models including F1/3, A1, A2, P1/3 and P1/4 models for AP thermal decomposition with Cu_2O, Cu_2O-C_{60} and Al-Cu_2O-C_{60} catalysts, and Avrami–Erofeev Equation (A1 and A3/2 models) for AP, AP-CuC_2O_4 and AP-ZnC_2O_4 systems.[65]

3.5 Thermal Decomposition Mechanism of AP Supplemented with CuO NPs

The thermal decomposition of AP is complex, and numerous investigations, which have been undertaken to elucidate its whole decomposition mechanism, agree well that AP thermal decomposition starts with an allotropic transition around 240 °C, followed by a low temperature decomposition and high temperature decomposition HTD with an intermediate thermal decomposition ITD in some studies. One of the most important reasons of this difference of mechanism is the complexity and the poor reproductively of the determination of the conductivity of ammonium perchlorate using different tools.[66] On the basis of several investigations, *Boldyrev*[6] has assumed that AP thermal decomposition sustains with proton transfer from NH_4^+ to ClO_4^- according to the Scheme proposed by Jakobs, where "a" denotes the adsorbed phase and "g" gas phase.

$$NH_4ClO_4 \rightarrow NH_3\text{-}H\text{-}ClO_4 \rightarrow NH_3\text{-}HClO_4 \rightarrow NH_{3(a)} + HClO_{4(a)}\ (LTD) \rightarrow NH_{3(g)} + HClO_{4(g)}\ (HTD) \quad (5)$$

Based on these research works, and the evolved gases from the thermal decomposition of AP reviewed by *Benhammada* and *Trache*,[37c] the catalytic action of the added copper oxide nanoparticles could be assigned to the proton transfer. It is believed that the solid phase reaction occurs at the interface of the catalyst and the dispersed CuO on AP matrix leads to the production of more heat release, and hence accelerates the decomposition process with lower temperature.[67] AP decomposes following two steps. During the first one, the ammonia oxidation is promoted with a proton transfer. The O^{2-} species formed during AP decomposition and the surface O^{2-} species of CuO are likely the proton traps according to Equation (6):[34a]

$$2NH_4^+ + O^{2-} \rightarrow H_2O + 2NH_3 \quad (6)$$

On other hand, CuO is a narrow bandgap p-type semiconductor material (1.68 eV), with a concentration of free holes (h^+) on valence band (VB) of 1.40 eV and electron (e^-) on conduction band (CB) of –1.30 eV. It is considered very conductive to the thermal decomposition of AP.[17] At HTD decomposition, the excitation energy is higher to the bandgap and the band potential (0.46 eV), and hence the CB electron (e-) and VB holes are formed ,[61] which can react with the adsorbed $HClO_4$ on the Cu^{2+} surfaces, forming promptly the super-oxide radical anion O^{2-} [Equation (7)]. The association of O^{2-} and h^+ could further assist NH_3 to decompose, generating NO_2, N_2O, O_2, H_2O and N_2.[10a,68]

$$HClO_4 + e^- \rightarrow HClO_3 + O^- \quad (7)$$

The perchloric acid decomposes as well and leads to the formation of HCl, ClO, ClO_3, H_2O, O_2, Cl_2, and H_2O[5c,10a,60] (Figure 9).

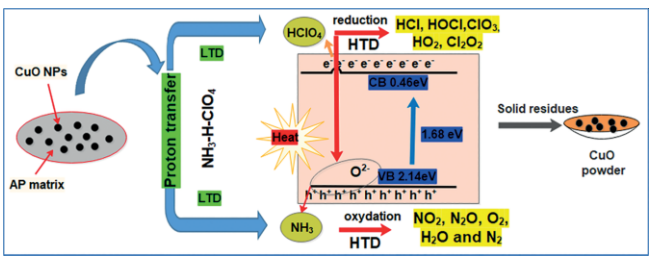

Figure 9. Illustration of catalytic action of CuO NPs on thermal decomposition of AP.

4 Conclusions

The experiments described in this work show the application of green CuO nanoparticles produced from different precursors as catalysts of the thermal decomposition of ammonium perchlorate. CuO nanoparticles have been synthesized by a precipitation method using three copper precursors and Malva sylvestris leaf aqueous extract as a capping agent. The obtained CuO-NPs exhibit pure chemical composition with a spherical shape.

From the thermal analysis of the AP/CuO NPs, it is found that the presence of CuO NPs decreases the thermal decomposition temperature, which occurred as a one-step. Besides that, compared to pure AP, the incorporation of CuO NPs reduces the HTD temperature by 91.7, 89.9, and 83 °C for CuO-S, CuO-N and CuO-Cl, respectively. Furthermore, the amount of exothermic enthalpy was significantly increased by 1053, 962, and 832 $J{\cdot}g^{-1}$ for AP-CuO-S, AP-CuO-Cl, and AP-CuO-N, respectively, exhibiting the good catalytic effect of the added catalysts on thermal decomposition of AP.

It is also revealed that the activation energy is reduced through the incorporation CuO NPs, with a lower value for AP-CuO-S system, demonstrating that the nature of precursor used to produce catalysts may affect the decomposition process of AP. Moreover, the most probable decomposition mechanisms [g(α)] was determined using it-KAS, it-FWO and TAS models. Based on it-KAS and it-FWO methods, AP decomposes according to different mechanisms. While at LTD stage, AP decomposes following F1/3 model chemical reaction with n^{th} (n = 2/3) reaction order, the HTD stage is governed by

P1/2 model [$g(\alpha) = \alpha^{1/2}$], which belongs to a nucleation (Power low). After the addition of the MO nanoparticles, TAS method provides the same G7 and G8 for pure AP at LTD, AP-CuO-Cl and AP-CuO-N, whereas, F1/3 models or F1/2 contracting cylinder for AP-CuO-S, and P1/4 model [$g(\alpha) = \alpha^{1/4}$] for pure AP at HTD are found. An attempt to discuss the catalytic effect of CuO NPs on the mechanism of the thermal decomposition of AP with a schematic illustration has also been performed. Finally, we can deduce that the developed catalysts are potential candidates as ballistic modifiers for AP-based composite propellants.

Keywords: Ammonium perchlorate; CuO; Nanoparticles; Thermal decomposition; Kinetic parameters; Catalytic activity

References

[1] a) H. M. Pandas, M. Fazli, *J. Therm. Anal. Calorim.* **2018**, *131*, 2913–2924; b) D. Trache, F. Maggi, I. Palmucci, L. T. DeLuca, K. Khimeche, M. Fassina, S. Dossi, G. Colombo, *Arabian J. Chem.* **2019**, *12*, 3639–3651; c) D. Trache, F. Maggi, I. Palmucci, L. T. DeLuca, *J. Therm. Anal. Calorim.* **2018**, *132*, 1601–1615.
[2] D. Trache, T. M. Klapötke, L. Maiz, M. Abd-Elghany, L. T. DeLuca, *Green Chem.* **2017**, *19*, 4711–4736.
[3] a) P. W. M. Jacobs, H. Whitehead, *Chem. Rev.* **1969**, *69*, 551–590; b) T. Urbanski, S. Laverton, W. Ornaf, *Chemistry and technology of explosives, Vol. 1*, Pergamon Press New York, NY, **1964**.
[4] a) G. P. Sutton, O. Biblarz, *Rocket propulsion elements*, John Wiley & Sons, **2016**; b) A. Mezroua, K. Khimeche, M. H. Lefebvre, M. Benziane, D. Trache, *J. Therm. Anal. Calorim.* **2014**, *116*, 279–286; c) A. Mezroua, M. H. Lefebvre, D. Trache, K. Khimeche, in *Innovative Energetic Materials: Properties, Combustion Performance and Application*, Springer, **2020**, pp. 351–372.
[5] a) Y. Ramdani, Q. Liu, G. Huiquan, P. Liu, A. Zegaoui, J. Wang, *Vacuum* **2018**, *153*, 277–290; b) I. P. S. Kapoor, P. Srivastava, G. Singh, *Propellants Explos. Pyrotech.* **2009**, *34*, 351–356; c) L. Mallick, S. Kumar, A. Chowdhury, *Thermochim. Acta* **2015**, *610*, 57–68.
[6] V. Boldyrev, *Thermochim. Acta* **2006**, *443*, 1–36.
[7] Y.-L. Zhu, H. Huang, H. Ren, Q.-J. Jiao, *J. Energetic. Mater.* **2014**, *32*, 16–26.
[8] Q. Li, Y. He, R. Peng, *RSC Adv.* **2015**, *5*, 24507–24512.
[9] Q.-L. Yan, F.-Q. Zhao, K. K. Kuo, X.-H. Zhang, S. Zeman, L. T. DeLuca, *Prog. Energy Combustion Science* **2016**, *57*, 75–136.
[10] a) T. Chen, P. Du, W. Jiang, J. Liu, G. Hao, H. Gao, L. Xiao, X. Ke, F. Zhao, C. Xuan, *RSC Adv.* **2016**, *6*, 83838–83847; b) A. Benhammada, D. Trache, M. Kesraoui, S. Chelouche, *Nanomaterials* **2020**, *10*, 968; c) A. Benhammada, D. Trache, M. Kesraoui, A. F. Tarchoun, S. Chelouche, A. Mezroua, *Thermochim. Acta* **2020**, 178570.
[11] a) Z. Cheng, X. Chu, J. Xu, H. Zhong, L. Zhang, *Ceramics Int.* **2016**, *42*, 3876–3881; b) J. Sharma, P. Srivastava, G. Singh, M. S. Akhtar, S. Ameen, *Thermochim. Acta* **2015**, *614*, 110–115; c) I. P. S. Kapoor, P. Srivastava, G. Singh, *Propellants Explos. Pyrotech.* **2009**, *34*, 351–356.
[12] a) L.-N. Jin, Q. Liu, W.-Y. Sun, *CrystEngComm* **2012**, *14*, 7721–7726; b) S. Lu, X. Jing, J. Liu, J. Wang, Q. Liu, Y. Zhao, S. Jamil, M. Zhang, L. Liu, *J. Solid State Chem.* **2013**, *197*, 345–351; c) Y. Zhao, X. Xu, Y. Zhao, H. Zhou, J. Li, H. Jin, *J. Alloys Compd.* **2016**, *654*, 523–528.
[13] Y. Wang, J. Zhu, X. Yang, L. Lu, X. Wang, *Thermochim. Acta* **2005**, *437*, 106–109.
[14] Y. Zhang, X. Liu, J. Nie, L. Yu, Y. Zhong, C. Huang, *J. Solid State Chem.* **2011**, *184*, 387–390.
[15] B. Wu, Y. Lai, X. Qi, H. Du, C. Pei, *ACS Appl. Energy Mater.* **2019**, *2*, 8319–8327.
[16] J. Xu, S. Li, L. Tan, B. Kou, *Mater. Res. Bull.* **2017**, *52*, 352–360.
[17] Q. Zhang, K. Zhang, D. Xu, G. Yang, H. Huang, F. Nie, C. Liu, S. Yang, *Prog. Mater. Science* **2014**, *60*, 208–337.
[18] L. Shi, X. Fu, C. Fan, S. Yu, G. Qian, Z. Wang, *RSC Adv.* **2015**, *5*, 85179–85186.
[19] M.-K. Song, S. Park, F. M. Alamgir, J. Cho, M. Liu, *Mater. Sci. Eng.* **2011**, *72*, 203–252.
[20] Z. H. Ibupoto, A. Tahira, H. Raza, G. Ali, A. A. Khand, N. S. Jilani, A. B. Mallah, C. Yu, M. Willander, *Materials* **2018**, *11*, 1378.
[21] C. Wang, W. Zeng, T. Li, Y. Li, *Mater. Technology* **2015**, *30*, 205–212.
[22] C. Yang, F. Xiao, J. Wang, X. Su, *J. Colloid Interface Sci.* **2014**, *435*, 34–42.
[23] C. Rossi, K. Zhang, D. Esteve, P. Alphonse, P. Tailhades, C. Vahlas, *J. Microelectromechanical Systems* **2007**, *16*, 919–931.
[24] T. H. Tran, V. T. Nguyen, *Int. Scholarly Res. Notices* **2014**, *2014*.
[25] a) V. V. T. Padil, M. Černík, *Int. J. Nanomedicine* **2013**, *8*, 889; b) P. V. Kumar, U. Shameem, P. Kollu, R. Kalyani, S. Pammi, *BioNanoScience* **2015**, *5*, 135–139; c) S. Gunalan, R. Sivaraj, R. Venckatesh, *Spectrochim. Acta Part A: Mol. Biomolecular. Spectrosc.* **2012**, *97*, 1140–1144.
[26] B. Xue, Z. Qian, C. Liu, G. Luo, *Russ. J. Appl. Chem.* **2017**, *90*, 138–143.
[27] J. Wang, S. He, Z. Li, X. Jing, M. Zhang, Z. Jiang, *J. Chem. Sci.* **2009**, *121*, 1077.
[28] E. Ayoman, S. G. Hosseini, *J. Therm. Anal. Calorim.* **2016**, *123*, 1213–1224.
[29] Y. Hu, S. Yang, B. Tao, X. Liu, K. Lin, Y. Yang, R. Fan, D. Xia, D. Hao, *Vacuum* **2019**, *159*, 105–111.
[30] T. Zhou, X. Qi, Y. Ma, C. Pei, X. Duan, B. Wu, *Appl. Organometallic Chem.* **2020**, e5730.
[31] a) S. Vyazovkin, *Isoconversional kinetics of thermally stimulated processes*, Springer, **2015**; b) S. Vyazovkin, A. K. Burnham, J. M. Criado, L. A. Pérez-Maqueda, C. Popescu, N. Sbirrazzuoli, *Thermochim. Acta* **2011**, *520*, 1–19.
[32] A. Umar, A. Alshahrani, H. Algarni, R. Kumar, *Sensors Actuators B: Chem.* **2017**, *250*, 24–31.
[33] S. Kim, A. Umar, R. Kumar, A. A. Ibrahim, G. Kumar, *Mater. Lett.* **2015**, *156*, 138–141.
[34] a) L. Chen, L. Li, G. Li, *J. Alloys Compd.* **2008**, *464*, 532–536; b) H. Siddiqui, M. Qureshi, F. Z. Haque, *Optik* **2016**, *127*, 4726–4730.
[35] M. Rashad, M. Rüsing, G. Berth, K. Lischka, A. Pawlis, *J. Nanomaterials* **2013**, *2013*.
[36] D. Das, B. C. Nath, P. Phukon, S. K. Dolui, *Colloids Surf. B: Biointerfaces* **2013**, *101*, 430–433.
[37] a) Y. Zhang, K. Li, J. Liao, X. Wei, L. Zhang, *Appl. Surf. Sci.* **2020**, *499*, 143875; b) S. Chaturvedi, P. N. Dave, *J. Saudi. Chem. Soc.* **2013**, *17*, 135–149; c) A. Benhammada, D. Trache, *Appl. Spectrosc. Rev.* **2020**, *55*, 725–777.
[38] L. Mallick, S. Kumar, A. Chowdhury, *Thermochim. Acta* **2017**, *653*, 83–96.
[39] L. Bircumshaw, B. H. Newman, *Proc. R. Soc. London Ser. A Mathematical. Phys. Sci.* **1954**, *227*, 115–132.
[40] B. Longuet, P. Gillard, *Propellants Explos. Pyrotech.* **2009**, *34*, 59–71.
[41] M. Mahdavi, H. Farrokhpour, M. Tahriri, *Mater. Chem. Phys.* **2017**, *196*, 9–20.
[42] Z. Jia, D. Ren, Q. Wang, R. Zhu, *Appl. Surf. Sci.* **2013**, *270*, 312–318.
[43] V. Mirzajani, K. Farhadi, S. M. Pourmortazavi, *J. Therm. Anal. Calorim.* **2018**, *131*, 937–948.
[44] T. An, F. Zhao, H. Gao, H. Ma, H. Hao, J. Yi, Y. Yang, *J. Mater. Eng.* **2011**, *1*, 23–28.
[45] J. Zhao, Z. Liu, Y. Qin, W. Hu, *CrystEngComm* **2014**, *16*, 2001–2008.

[46] M. Zou, X. Wang, X. Jiang, L. Lu, *J. Solid State Chem.* **2014**, *213*, 235–241.
[47] Y. Xu, D. Chen, X. Jiao, K. Xue, *Mater. Res. Bull.* **2007**, *42*, 1723–1731.
[48] S. G. Hosseini, Z. Khodadadipoor, M. Mahyari, *Appl. Organometal. Chem.* **2018**, *32*, e3959.
[49] A. Eslami, N. M. Juibari, S. G. Hosseini, *Mater. Chem. Phys.* **2016**, *181*, 12–20.
[50] S. G. Hosseini, S. J. H. Toloti, K. Babaei, A. Ghavi, *J. Therm. Anal. Calorim.* **2016**, *124*, 1243–1254.
[51] S. Vyazovkin, C. A. Wight, *Anal. Chem.* **2000**, *72*, 3171–3175.
[52] a) S. Vyazovkin, C. A. Wight, *Int. Rev. Phys. Chem.* **1998**, *17*, 407–433; b) S. Vyazovkin, *J. Therm. Anal. Calorim.* **2001**, *64*, 829–835.
[53] a) S. Chelouche, D. Trache, Z. I. Benayachi, A. F. Tarchoun, K. Khimeche, A. Mezroua, *Propellants Explos. Pyrotech.* **2020**; b) S. Chelouche, D. Trache, A. F. Tarchoun, A. Abdelaziz, K. Khimeche, *J. Energetic Mater.* **2019**, 1–20.
[54] F. Hayoune, S. Chelouche, D. Trache, S. Zitouni, Y. Grohens, *Thermochim. Acta* **2020**, *690*, 178700.
[55] Z. Gao, M. Nakada, I. Amasaki, *Thermochim. Acta* **2001**, *369*, 137–142.
[56] S. Vyazovkin, in *Isoconversional kinetics of thermally stimulated processes*, Springer, **2015**, pp. 1–25.
[57] D. Trache, A. Abdelaziz, B. Siouani, *J. Therm. Anal. Calorim.* **2017**, *128*, 335–348.
[58] S. Chelouche, D. Trache, A. F. Tarchoun, A. Abdelaziz, K. Khimeche, A. Mezroua, *Thermochim. Acta* **2019**, *673*, 78–91.
[59] D. Zhang, L. Jiang, S. Lu, C.-Y. Cao, H.-P. Zhang, *Fuel* **2018**, *217*, 553–560.
[60] Q.-J. Jiao, Y.-L. Zhu, J.-C. Xing, H. Ren, H. Huang, *J. Therm. Anal. Calorim.* **2014**, *116*, 1125–1131.
[61] G. Tang, S. Tian, Z. Zhou, Y. Wen, A. Pang, Y. Zhang, D. Zeng, H. Li, B. Shan, C. Xie, *J. Phys. Chem. C* **2014**, *118*, 11833–11841.
[62] a) M. F. Cherif, D. Trache, F. Benaliouche, A. F. Tarchoun, S. Chelouche, A. Mezroua, *Int. J. Biol. Macromolecules* **2020**, *164*, 794–807; b) M. F. Cherif, D. Trache, F. Benaliouche, S. Chelouche, A. F. Tarchoun, A. Mezroua, *Thermochim. Acta* **2020**, 178732.
[63] H. Zhang, P. Li, W. Cui, C. Liu, S. Wang, S. Zheng, Y. Zhang, *RSC Adv.* **2016**, *6*, 27235–27241.
[64] P. R. Patil, V. e. N. Krishnamurthy, S. S. Joshi, *Propellants Explos. Pyrotech.* **2008**, *33*, 266–270.
[65] M. Mahdavi, H. Farrokhpour, M. Tahriri, *J. Therm. Anal. Calorim.* **2018**, *132*, 879–893.
[66] F. Solymosi, *Structure and stability of salts of halogen oxyacids in the solid phase*, Wiley, **1977**.
[67] M. Zou, X. Jiang, L. Lu, X. Wang, *J. Hazard. Mater.* **2012**, *225*, 124–130.
[68] S. Yang, C. Wang, L. Chen, S. Chen, *Mater. Chem. Phys.* **2010**, *120*, 296–301.

Received: August 9, 2020
Published Online: ■

Journal of Inorganic and General Chemistry
ZAAC
Zeitschrift für anorganische und allgemeine Chemie

ARTICLE